


## Non-Hermitian Floquet topological phases in the double-kicked rotor

Longwen Zhou<sup>✉\*</sup> and Jiaxin Pan

*Department of Physics, College of Information Science and Engineering, Ocean University of China, Qingdao 266100, China*

 (Received 8 August 2019; published 11 November 2019)

Dynamical kicking systems possess rich topological structures. In this work we study Floquet states of matter in a non-Hermitian extension of the double-kicked rotor model. Under the on-resonance condition, we find various non-Hermitian Floquet topological phases, each being characterized by a pair of topological winding numbers. A generalized mean chiral displacement is introduced to detect these winding numbers dynamically in two symmetric time frames. Furthermore, by mapping the system to a periodically quenched lattice model, we obtain the topological edge states and unravel the bulk-edge correspondence of the non-Hermitian double-kicked rotor. These results reveal the richness of Floquet topological states in non-Hermitian dynamical kicking systems.

DOI: [10.1103/PhysRevA.100.053608](https://doi.org/10.1103/PhysRevA.100.053608)

### I. INTRODUCTION

Floquet topological phases of matter emerge in systems under time-periodic modulations. One class of Floquet systems that has been shown to possess rich topological properties is dynamical kicking systems [1]. They were first introduced in the study of dynamical localization and quantum chaos, with the kicked rotor (KR) being a prototypical example [2–7]. Wang and Gong analyzed a modified version of the KR (called the double-kicked rotor) [8] and discovered its fractal quasienergy spectrum that mimics the Hofstadter butterfly in quantum Hall effects [9]. Later, rich Floquet topological states in the double-kicked rotor (DKR) were characterized and then employed to achieve quantized acceleration in momentum space [10]. The topological equivalence between the DKR and the kicked Harper model [11], another prototypical dynamical kicking system, has also been proved rigorously [12]. The introduction of a spin-1/2 degree of freedom to the KR and DKR further reveals the richness of Floquet topological states that can appear in dynamical kicking systems [13–15].

In the past decade, Floquet topological phases have attracted a great deal of interest across a broad range of research areas. This is mainly due to the richness and high-tunability of their topological properties [16–44], with potential applications in ultrafast electronics [45], quantum simulation [46], and quantum computing [47]. The topological classification of these dynamical states of matter also requires new schemes [48–50] that go beyond their static cousins. Experimentally, Floquet topological phases have been realized in cold-atom, photonic, phononic, and acoustic systems [51–57].

In recent years, the study of Floquet topological phases has been extended to the non-Hermitian domain [58,59]. There, gain and loss or nonreciprocal effects were introduced to make the evolution of Floquet systems nonunitary [60–64]. In quantum walk setups, gain and loss were implemented in several studies to measure the topological invariants [65–73]. Furthermore, a periodically quenched nonreciprocal lattice model has been found to possess abundant Floquet topological

phases with arbitrarily many topological edge states induced by non-Hermitian effects [74]. In dynamical kicking systems, a  $\mathcal{PT}$ -symmetric kicked rotor was proposed [75,76] and its transport properties were investigated in [77]. However, none of these works revealed the richness of non-Hermitian Floquet topological phases in dynamical kicking systems.

In this work we introduce a DKR with complex kicking strengths and unravel its fruitful non-Hermitian Floquet topological phases. After introducing our model in Sec. II, we analyze its spectrum, symmetry, and topological properties in Sec. III. A pair of integer winding numbers is introduced to fully characterize the topological phases appearing in the non-Hermitian DKR. We further extend the definition of mean chiral displacement (MCD) to nonunitary evolution and use it as a probe to extract the topological winding numbers of the non-Hermitian DKR dynamically. By mapping our system to a periodically kicked lattice model, we also present its topological edge states under an open boundary condition (OBC) and demonstrate its bulk-edge correspondence. We summarize our work and discuss potential future directions in Sec. IV.

### II. MODEL

The DKR model is described by the Hamiltonian  $\hat{H} = \frac{\hat{p}^2}{2} + \kappa_1 \cos(\hat{x} + \beta) \sum_{\ell \in \mathbb{Z}} \delta(t - \ell T) + \kappa_2 \cos(\hat{x}) \sum_{\ell \in \mathbb{Z}} \delta(t - \ell T - \tau)$ . It can be realized by cold atoms subject to counterpropagating laser pulses in an optical lattice [78–80], where  $\hat{x}$  and  $\hat{p}$  are position and momentum operators of cold atoms. In a driving period  $T$ , the system is first kicked by a lattice potential of strength  $\kappa_1$ . Then it is evolved freely over a time duration  $\tau \in (0, T)$ , kicked by another lattice potential of strength  $\kappa_2$ , and then evolved freely over another time duration  $T - \tau$ . In addition,  $\beta$  is a controllable phase shift between the two kicking potentials. The Floquet operator of the DKR, obtained by integrating the Schrödinger equation  $i\hbar\partial_t|\psi\rangle = \hat{H}|\psi\rangle$  over a complete driving period, e.g., from  $t = \ell T - 0^+$  to  $t = (\ell + 1)T - 0^+$ , is given by

$$\hat{U} = e^{-i(T-\tau)(\hat{p}^2/2\hbar)} e^{-i(\kappa_2/\hbar)\cos(\hat{x})} e^{-i\tau(\hat{p}^2/2\hbar)} e^{-i(\kappa_1/\hbar)\cos(\hat{x}+\beta)}. \quad (1)$$

\*zhoulw13@u.nus.edu

In the Floquet operator, the spatial periodicity of kicking potentials allows the momentum  $\hat{p}$  to take eigenvalues  $p = (n + \eta)\hbar$ , where  $n \in \mathbb{Z}$  and  $\eta \in (0, 1)$  are the conserved quasi-momenta. For a Bose-Einstein condensate of large coherence width, one can choose  $\eta = 0$  [81,82]. The momentum  $\hat{p}$  is then quantized as  $\hat{p} = \hat{n}\hbar$ , i.e., integer multiples of the effective Planck constant  $\hbar$ . Furthermore, under the condition  $\hbar T = 4\pi$  [81–83], we obtain the on-resonance DKR (ORDKR) model, whose Floquet operator takes the form

$$\hat{U} = e^{+i(\hbar\tau/2)\hat{n}^2} e^{-iK_2 \cos(\hat{x})} e^{-i(\hbar\tau/2)\hat{n}^2} e^{-iK_1 \cos(\hat{x}+\beta)}. \quad (2)$$

Here  $K_1 = \kappa_1/\hbar$  and  $K_2 = \kappa_2/\hbar$  represent dimensionless kicking strengths. It has been shown that this ORDKR model possesses rich topological properties, including the Hofstadter butterflylike Floquet spectrum [8], quasienergy bands with large Chern numbers, and quantized Thouless pumping in momentum space [10].

In this work we further investigate the Floquet topological phases of the ORDKR in the non-Hermitian regime. More specifically, we focus on the two-band situation by choosing the time delay  $\tau$  between the two kicks such that  $\hbar\tau = \pi$ . The resulting non-Hermitian (NH) ORDKR model is described by the Floquet operator

$$\hat{U} = e^{i(\pi/2)\hat{n}^2} e^{-iK_2 \cos(\hat{x})} e^{-i(\pi/2)\hat{n}^2} e^{-iK_1 \cos(\hat{x}+\beta)}, \quad (3)$$

where the kicking strengths

$$K_j = u_j + iv_j, \quad j = 1, 2, \quad (4)$$

now take complex values, with  $\{u_1, v_1, u_2, v_2\} \in \mathbb{R}$ . For an optical lattice, the imaginary parts of kicking strengths correspond to particle losses, which may be generated by using a resonant optical beam to kick the atoms out of the trap. They may also be realized by applying a radio-frequency pulse to excite atoms to an irrelevant state, leading to an effective decay when atoms in that state experience a loss by applying an antitrap [84]. In photonic systems, a complex kicking strength corresponds to a complex refractive index, whose imaginary part represents either loss or gain. This kind of potential has interesting engineering applications, such as realizing unidirectional transport of light [85] and other types of laser devices [63]. In the following, we will unravel rich Floquet topological phases in the NH ORDKR induced by complex kicking lattice potentials.

### III. FLOQUET TOPOLOGICAL PHASES IN THE NH ORDKR

In this section we first analysis the Floquet operator of the NH ORDKR in Eq. (3) and discuss the symmetry that protects its topological properties. Next we investigate the quasienergy spectrum and the conditions of topological phase transitions in the NH ORDKR. A pair of integer topological winding numbers is introduced to characterize each of its Floquet topological phases. To detect these winding numbers and distinguish different Floquet topological phases in the NH ORDKR experimentally, we suggest the measurement of the MCD of a wave packet in the optical lattice. Finally, we map the Floquet operator of the NH ORDKR to a kicked lattice model in the position representation and uncover its Floquet edge states and bulk-edge correspondence under an OBC.

#### A. Floquet operator and chiral symmetry

The Floquet operator of the NH ORDKR, as defined in Eq. (3), is translationally invariant over two sites, i.e.,  $\hat{n} \rightarrow \hat{n} + 2$ , in the momentum lattice. By introducing a bipartite lattice basis in momentum space and taking the periodic boundary condition, we could express the Floquet operator of the NH ORDKR as  $\hat{U} = \sum_{\theta} U(\theta)|\theta\rangle\langle\theta|$ , where

$$U(\theta) = e^{+i(\pi/4)\sigma_z} e^{-iK_2[\cos(\theta/2)\sigma_x + \sin(\theta/2)\sigma_y]} \times e^{-i(\pi/4)\sigma_z} e^{+iK_1[\cos(\theta/2)\sigma_x + \sin(\theta/2)\sigma_y]}, \quad (5)$$

with

$$\mathcal{K}_1 \equiv K_1 \sin \frac{\theta}{2}, \quad \mathcal{K}_2 \equiv K_2 \cos \frac{\theta}{2}, \quad (6)$$

$\theta \in [-\pi, \pi)$  being the conserved quasiposition due to translational symmetry in momentum space, and  $\sigma_{x,y,z}$  being Pauli matrices in their usual representation [see Appendix A for derivation details of Eq. (5)]. We have also set the phase delay between two kicks to be  $\beta = \frac{\pi}{2}$ , which allows  $U(\theta)$  to possess nontrivial topological phases when  $K_{1,2}$  takes real values [10].

To characterize the symmetry and topological properties of  $U(\theta)$ , we introduce a pair of symmetric time frames by resetting the start time of the evolution. In these time frames,  $U(\theta)$  takes the form

$$U_1(\theta) = e^{-i(\mathcal{K}_2/2)[\cos(\theta/2)\sigma_x + \sin(\theta/2)\sigma_y]} e^{-i\mathcal{K}_1[\sin(\theta/2)\sigma_x - \cos(\theta/2)\sigma_y]} \times e^{-i(\mathcal{K}_2/2)[\cos(\theta/2)\sigma_x + \sin(\theta/2)\sigma_y]}, \quad (7)$$

$$U_2(\theta) = e^{+i(\mathcal{K}_1/2)[\cos(\theta/2)\sigma_x + \sin(\theta/2)\sigma_y]} e^{-i\mathcal{K}_2[\sin(\theta/2)\sigma_x - \cos(\theta/2)\sigma_y]} \times e^{+i(\mathcal{K}_1/2)[\cos(\theta/2)\sigma_x + \sin(\theta/2)\sigma_y]}. \quad (8)$$

Note that both  $U_1(\theta)$  and  $U_2(\theta)$  are similar to  $U(\theta)$  (see Appendix A for more details). Therefore, they share the same Floquet spectrum with  $U(\theta)$  even if  $K_1$  and  $K_2$  are complex numbers. Furthermore, under the unitary transformation  $\Gamma = \sigma_z$ , we have

$$\Gamma U_{\alpha}(\theta) \Gamma = U_{\alpha}^{-1}(\theta), \quad \alpha = 1, 2, \quad (9)$$

which means that  $U_1(\theta)$  and  $U_2(\theta)$  have the chiral (sublattice) symmetry  $\Gamma$ . According to the symmetry classification of chiral symmetric Floquet systems in one dimension [39] and its extension to non-Hermitian systems [74], each topological phase of  $U(\theta)$  can be described by a pair of integer winding numbers extracted from  $U_1(\theta)$  and  $U_2(\theta)$ . We will analyze the spectrum and topological properties of the NH ORDKR in detail in the following sections.

#### B. Quasienergy dispersion, topological invariants, and phase diagram

Expanding  $U_1(\theta)$  and  $U_2(\theta)$  by the Euler formula and recombining the resulting terms, we can express Eqs. (7) and (8) in a compact form as

$$U_{\alpha}(\theta) = e^{-iE(\theta)(n_{\alpha x}\sigma_x + n_{\alpha y}\sigma_y)}, \quad (10)$$

where  $\alpha = 1, 2$  and

$$E(\theta) = \arccos(\cos \mathcal{K}_1 \cos \mathcal{K}_2) \quad (11)$$

gives the quasienergy dispersion relation  $\pm E(\theta)$ . Since the real part of  $E(\theta)$  is only defined modulus  $2\pi$ , the quasienergy spectral gap closes when  $\text{Im}E(\theta) = 0$  and  $\text{Re}E(\theta) = 0$  or  $\pm\pi$ . When the spectrum becomes gapless, a topological phase transition may happen. Furthermore,  $(n_{\alpha x}, n_{\alpha y})$  forms a complex-valued vector with  $n_{\alpha x}^2 + n_{\alpha y}^2 = 1$  for  $\alpha = 1, 2$  (see Appendix B for more details). Using these vectors, we can define a winding number for  $U_\alpha(\theta)$  as

$$v_\alpha = \int_{-\pi}^{\pi} \frac{d\theta}{2\pi} (\mathbf{n}_\alpha \times \partial_\theta \mathbf{n}_\alpha)_z, \quad \alpha = 1, 2. \quad (12)$$

It is not hard to see that  $v_\alpha$  take real values, as the imaginary part of  $\mathbf{n}_\alpha \equiv (n_{\alpha x}, n_{\alpha y})$  has no winding in the Brillouin zone [74]. Then, following the description of chiral symmetric non-Hermitian Floquet systems [74], the topological phases of  $U(\theta)$  can be characterized by a pair of integer winding numbers, given by<sup>1</sup>

$$v_0 = \frac{v_1 + v_2}{2}, \quad v_\pi = \frac{v_1 - v_2}{2}. \quad (13)$$

In the Hermitian limit (imaginary parts of the two kicking strengths  $v_1 = v_2 = 0$ ),  $v_0$  and  $v_\pi$  also predict the number of topological edge modes at quasienergy zero and  $\pi$  in the ORDKR model [10].

In the following, we will analyze the spectrum and topological phases of ORDKR under three representative non-Hermitian kicking potentials: (i)  $v_1 \neq 0$  and  $v_2 = 0$  or vice versa, (ii)  $v_1 = v_2 = v \neq 0$ , and (iii)  $v_1 \neq v_2$  with  $v_1, v_2 \neq 0$ . In each case, we give the condition of topological phase transition, computing winding numbers for each of the topological phases and constructing the corresponding topological phase diagram.

### 1. Case (i)

We first consider the case when only one of the kicking strengths ( $K_1$  or  $K_2$ ) in Eq. (4) is complex. Under the gapless condition  $\cos[E(\theta)] = \pm 1$ , it can be shown that if  $v_1 \neq 0$  and  $v_2 = 0$ ,  $u_1$ ,  $u_2$ , and  $v_1$  in Eq. (4) satisfy the equation (see Appendix C for derivation details)

$$v_1 = \frac{u_1}{n\pi} \operatorname{arccosh} \left[ \frac{\pm 1}{\cos(u_2 \sqrt{1 - \frac{n^2 \pi^2}{u_1^2}})} \right], \quad n \in \mathbb{Z}. \quad (14)$$

Similarly, if  $v_2 \neq 0$  and  $v_1 = 0$ , the gapless condition yields

$$v_2 = \frac{u_2}{n\pi} \operatorname{arccosh} \left[ \frac{\pm 1}{\cos(u_1 \sqrt{1 - \frac{n^2 \pi^2}{u_2^2}})} \right], \quad n \in \mathbb{Z}. \quad (15)$$

Note that Eqs. (14) and (15) are symmetric under the exchange of subindices  $1 \leftrightarrow 2$ . So we can focus on the non-Hermitian Floquet topological phases and phase transitions related to only one of them without loss of generality.

<sup>1</sup>In calculations, we take absolute values on the right-hand side of Eq. (13) to compute  $(v_0, v_\pi)$ . In a topological sense,  $v_0 = \pm 1$  do not distinguish two different topological phases. The sign of the winding number could depend on the choice of conventions.

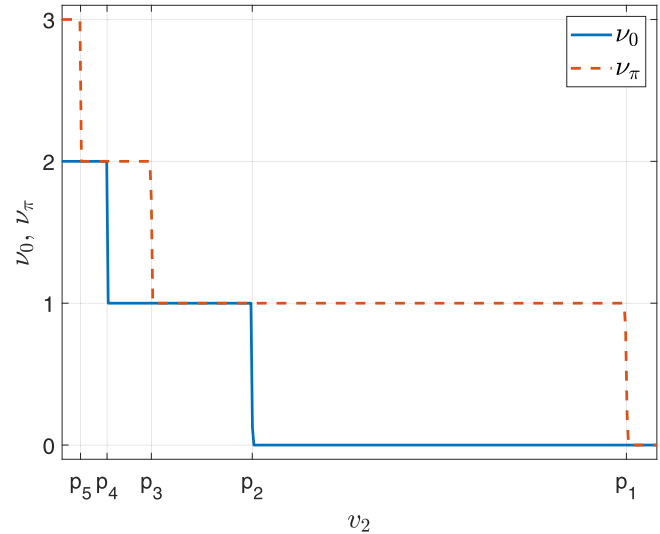


FIG. 1. Evolution of the winding numbers  $v_0$  (blue solid line) and  $v_\pi$  (red dashed line) vs the imaginary part of the kicking strength  $K_2 = u_2 + iv_2$ . The system parameters are chosen as  $u_1 = 0.5\pi$ ,  $u_2 = 5.5\pi$ , and  $v_1 = 0$ . The numerical values of  $p_1, p_2, p_3, p_4$ , and  $p_5$  along the  $v$  axis are obtained analytically from Eq. (15) with  $n = 1, 2, 3, 4, 5$ .

To check whether a nonvanishing imaginary part of  $K_1$  or  $K_2$  could induce new topological phases in the NH ORDKR, we need to investigate the behavior of winding numbers (12) versus this imaginary part. A representative example is shown in Fig. 1, where we choose  $u_1 = 0.5\pi$  and  $u_2 = 5.5\pi$  for the real parts of kicking strengths. According to Ref. [10], this choice leads to a Floquet topological phase with  $(v_0, v_\pi) = (2, 3)$  in the Hermitian limit. In Fig. 1 we observe that with the increase of imaginary kicking strength  $v_2$ , a series of topological phase transitions happens at  $v_2 = p_n$ , with  $n = 1, \dots, 5$  in Eq. (15). Each transition is accompanied by the vanishing of a spectral gap, together with the quantized change of winding number  $v_0$  (blue solid line) or  $v_\pi$  (red dashed line) by 1. In the limit  $v_2 \rightarrow \infty$ , the system ends in a topologically trivial phase with  $v_0 = v_\pi = 0$ .

Therefore, we conclude that a nonvanishing imaginary part in the kicking strength  $K_1$  or  $K_2$  of the NH ORDKR could indeed induce topological phase transitions and create non-Hermitian Floquet topological phases, with each characterized by a pair of integer quantized winding numbers  $(v_0, v_\pi)$ . In more general situations, analytical solutions for the gap closing conditions like Eqs. (14) and (15) may not be available. We will consider these cases in the following.

### 2. Case (ii)

In this case, both kicking strengths  $K_1$  and  $K_2$  take complex values under the constraint that their imaginary parts are equal, i.e.,  $v_1 = v_2 = v$ . Using the gapless condition (see Appendix C for more details) and the winding numbers  $(v_0, v_\pi)$ , we could then numerically characterize the Floquet topological phases of the NH ORDKR at different imaginary kicking strength  $v$ . Two representative examples will be discussed in the following.

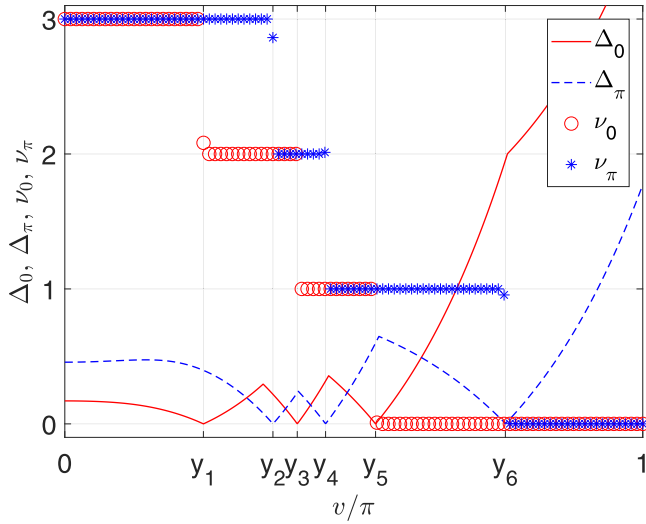


FIG. 2. Evolution of quasienergy gap functions  $\Delta_0$  (red solid line) and  $\Delta_\pi$  (blue dashed line) [see Eqs. (C8) and (C9) for the definitions] and winding numbers  $\nu_0$  (red circles) and  $\nu_\pi$  (blue stars) vs the imaginary parts of kicking strengths  $K_1 = u_1 + iv$  and  $K_2 = u_2 + iv$ . The system parameters are chosen as  $u_1 = 6.5\pi$  and  $u_2 = 0.5\pi$ . The numerical values of  $y_1, y_3$ , and  $y_5$  ( $y_2, y_4$ , and  $y_6$ ) along the  $v$  axis are obtained by searching for the local minimum of the gap function  $\Delta_0$  ( $\Delta_\pi$ ) around quasienergy  $E = 0$  ( $E = \pi$ ).

In the first example, we choose  $u_1 = 6.5\pi$  and  $u_2 = 0.5\pi$  for the real parts of two kicking strengths. When  $v = 0$ , the system is in a Hermitian Floquet topological phase with  $\nu_0 = \nu_\pi = 3$ . As shown in Fig. 2, increasing the imaginary kicking strength  $v$  yields consecutive Floquet topological phase transitions. Each transition happens when one of the gap functions ( $\Delta_0, \Delta_\pi$ ) [see Eqs. (C8) and (C9)] vanishes, accompanied by a quantized change of  $\nu_0$  or  $\nu_\pi$  by 1. In the limit  $v \rightarrow \infty$ , the system becomes topologically trivial, with  $\nu_0 = \nu_\pi = 0$ . Similar patterns of topological phase transitions are observed by exchanging the values of  $u_1$  and  $u_2$  for the two kicking strengths.

In the second example, we take  $u_1 = u_2 = u$ , which further indicates that  $K_1 = K_2$ . Plugging this condition into Eq. (13), we will always have  $\nu_1 = \nu_2$ . Therefore, we can obtain the topological phase diagram of the NH ORDKR versus  $u$  and  $v$ , with each phase characterized only by  $\nu_0$ . A representative portion of the phase diagram is shown in Fig. 3. Interestingly, we see that the increase of both  $u$  and  $v$  could induce topological phase transitions in the NH ORDKR. This further reveals the possibility of generating rich Floquet topological states in the ORDKR by complex kicking potentials.

3. Case (iii)

In this case, we allow both  $K_1$  and  $K_2$  to be complex, with no constraint on their imaginary parts. The resulting topological phase diagrams versus  $v_1$  and  $v_2$ , with  $(u_1, u_2) = (0.5\pi, 5.5\pi)$  and  $(u_1, u_2) = (5.5\pi, 0.5\pi)$ , are shown in Figs. 4 and 5, respectively. In each phase diagram, panels (a) and (b) correspond to the values of winding numbers  $\nu_0$  and  $\nu_\pi$ , respectively. A region with a uniform color refers to a parameter domain in which  $\nu_0$  [Figs. 4(a) and 5(a)] and  $\nu_\pi$

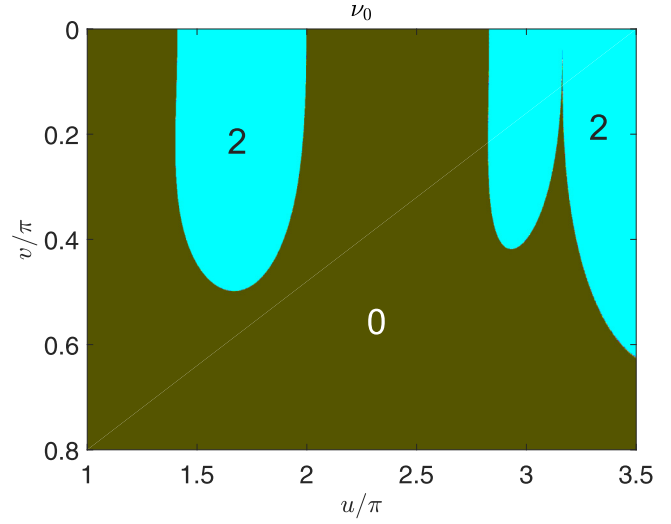


FIG. 3. Topological phase diagram of the NH ORDKR vs real and imaginary parts of kicking strengths  $K_1 = K_2 = u + iv$ . Each region with a uniform color corresponds to a Floquet topological phase of the NH ORDKR, with the numerical value of the winding number  $\nu_0$  shown in the figure.

[Figs. 4(b) and 5(b)] take the same value. We see that with the change of  $v_1$  and  $v_2$ , a couple of non-Hermitian Floquet topological phases are induced, with each characterized by the winding numbers ( $\nu_0, \nu_\pi$ ). Across the boundary between two topological phases, a quantized change of  $\nu_0$  or  $\nu_\pi$  is observed, which indicates the existence of a topological phase transition.

To sum up, we find that topological phase transitions are generic in the NH ORDKR model and rich non-Hermitian

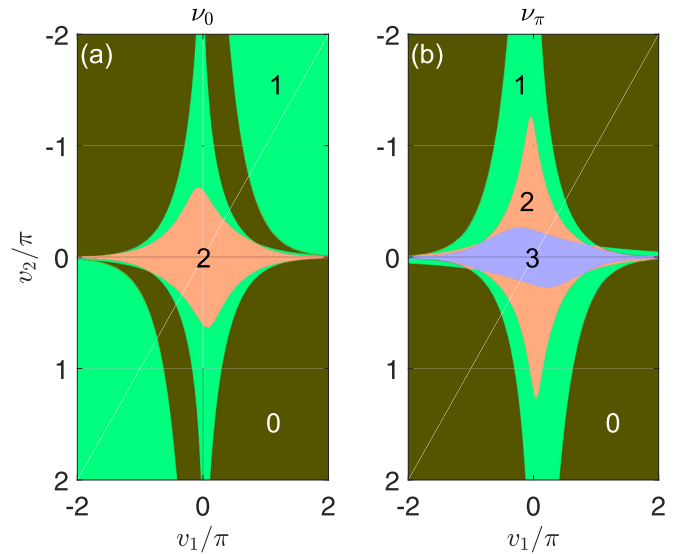


FIG. 4. Topological phase diagram of the NH ORDKR vs imaginary parts of kicking strengths  $K_1 = u_1 + iv_1$  and  $K_2 = u_2 + iv_2$ . The system parameters are chosen as  $u_1 = 0.5\pi$  and  $u_2 = 5.5\pi$ . Each region with a uniform color corresponds to a Floquet topological phase of the NH ORDKR, with the numerical values of winding numbers (a)  $\nu_0$  and (b)  $\nu_\pi$  shown.

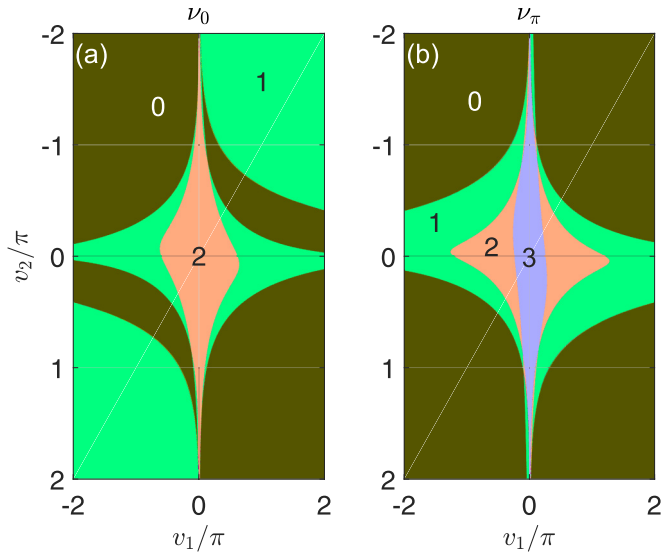


FIG. 5. Topological phase diagram of the NH ORDKR vs imaginary parts of kicking strengths  $K_1 = u_1 + iv_1$  and  $K_2 = u_2 + iv_2$ . The system parameters are chosen as  $u_1 = 5.5\pi$  and  $u_2 = 0.5\pi$ . Each region with a uniform color corresponds to a Floquet topological phase of the NH ORDKR, with the numerical values of winding numbers (a)  $\nu_0$  and (b)  $\nu_\pi$  shown.

Floquet topological phases could emerge under the effect of complex kicking potentials. In the following section we introduce a dynamical indicator, the MCD, to detect the winding numbers of these non-Hermitian Floquet topological phases.

### C. MCD and winding numbers

The MCD describes the shift of a localized wave packet in a bipartite lattice over a long-time duration. It was proposed as a way to detect the winding numbers of chiral symmetric topological insulators in one dimension [86,87]. In later studies, the MCD was applied to extract the winding numbers of Floquet systems [15] and was extended to two-dimensional systems with higher-order topological states [88]. In this work we generalize the MCD to non-Hermitian chiral symmetric Floquet systems and use it as a dynamical probe of the winding numbers of the NH ORDKR.

For a non-Hermitian Floquet system with chiral symmetry  $\Gamma$ , we define the chiral displacement as

$$C_\alpha(t) \equiv \text{Tr}[\rho_0 \hat{U}_\alpha^{\dagger t} (\hat{n} \otimes \Gamma) \hat{U}_\alpha^t], \quad (16)$$

where  $\alpha = 1, 2$  is the index of a symmetric time frame,  $t$  is the number of driving periods, and  $\hat{n}$  is the unit cell position operator (or momentum operator if the lattice is in momentum space). The initial state  $\rho_0 = \frac{|0\rangle\langle 0| \otimes \sigma_0}{2}$  describes a uniform mixture of sublattice eigenstates  $|a\rangle$  and  $|b\rangle$  in the 0's unit cell of the lattice. The choice of  $\rho_0$  here is different from the case in the Hermitian limit, in which the initial state occupies only a single sublattice in the 0's unit cell. Furthermore, the Floquet operator  $\hat{U}_\alpha$  is different from  $\hat{U}$  (the Floquet operator of the system in the  $\alpha$ 's time frame), in the sense that if  $|\psi\rangle$  is a right eigenvector of  $\hat{U}_\alpha$  with quasienergy  $E$ , then it is a left eigenvector of  $\hat{U}_\alpha$  with the same quasienergy.

With these definitions and after relatively straightforward calculations (see Appendix D for more details), the (normalized) MCD in the long-time limit is given by

$$\begin{aligned} \bar{C}_\alpha &= \lim_{t \rightarrow \infty} \frac{1}{t} \sum_{t'=1}^t \int_{-\pi}^{\pi} \frac{d\theta}{2\pi} \frac{(\mathbf{n}_\alpha \times \partial_\theta \mathbf{n}_\alpha)_z}{1 + |\cot(Et')|^2} \\ &= \frac{\nu_\alpha}{2}. \end{aligned} \quad (17)$$

Here  $\mathbf{n}_\alpha = (n_{\alpha x}, n_{\alpha y})$  is the winding vector of the Floquet operator in the  $\alpha$ 's time frame ( $\alpha = 1, 2$ ). For the NH ORDKR, explicit expressions of  $(n_{\alpha x}, n_{\alpha y})$  are given by Eqs. (B3)–(B6). Note that a normalization factor is introduced during the derivation of Eq. (17), which helps to cancel the effects of gain or loss on the amplitude of the evolving state. To reach the second equality of Eq. (17), we note that  $\frac{1}{1 + |\cot(Et')|^2} = \frac{1}{2} \{1 - \cos[2 \text{Re}(E)t'] / \cosh[2 \text{Im}(E)t']\}$ . When  $\text{Im}(E) = 0$ , we have an oscillating factor  $\frac{1}{2} \{1 - \cos[2 \text{Re}(E)t']\}$ , which will be averaged to  $\frac{1}{2}$  under  $\lim_{t \rightarrow \infty} \frac{1}{t} \sum_{t'=1}^t$ . When  $\text{Im}(E) \neq 0$ , the ratio  $\cos[2 \text{Re}(E)t'] / \cosh[2 \text{Im}(E)t']$  will approach 0 quickly at large  $t'$ , leaving only a factor  $\frac{1}{2}$  in  $\frac{1}{1 + |\cot(Et')|^2}$ . Therefore, we have  $\lim_{t \rightarrow \infty} \frac{1}{t} \sum_{t'=1}^t \frac{1}{1 + |\cot(Et')|^2} \rightarrow \frac{1}{2}$  and the other terms under the integral of Eq. (17) give nothing but the winding number  $\nu_\alpha$ . The winding numbers  $(\nu_0, \nu_\pi)$  can then be obtained from  $\bar{C}_\alpha$  as

$$\nu_0 = |\bar{C}_1 + \bar{C}_2|, \quad \nu_\pi = |\bar{C}_1 - \bar{C}_2|. \quad (18)$$

Importantly, even though the dispersion  $E(\theta)$  of the NH ORDKR is complex valued in general, the MCD as defined in Eq. (16) could still capture the topological winding numbers of the system dynamically, which emphasize its generality as a tool in probing non-Hermitian topological phases with chiral symmetry.

In Fig. 6 we show the winding numbers  $\nu_0$  (solid line) and  $\nu_\pi$  (dashed line) of the NH ORDKR calculated by the theoretical equations (12) and (13), together with  $|\bar{C}_1 + \bar{C}_2|$  ( $\bar{C}_0$  in the figure, denoted by circles) and  $|\bar{C}_1 - \bar{C}_2|$  ( $\bar{C}_\pi$  in the figure, denoted by triangles) calculated numerically by Eq. (17). Other system parameters are chosen as  $u_1 = 5.5\pi$ ,  $u_2 = 0.5\pi$ , and  $v_2 = 0$ . It is clear that the theoretical predictions of  $(\nu_0, \nu_\pi)$  and numerical results of MCD are consistent with each other, which verifies Eq. (18).

In Fig. 7 we give another example of MCD versus winding numbers, in which the system parameters are  $u_1 = 0.5\pi$  and  $u_2 = 6.5\pi$  and the imaginary parts of the two kicking strengths are equal. In this case, we again observe nice consistency between the MCD and winding numbers of the NH ORDKR within each of its topological phases. Therefore, we conclude that the MCD, as defined by Eq. (17), can be used as a generic probe of the topological winding numbers and topological phase transitions of one-dimensional non-Hermitian Floquet systems with chiral symmetry. To detect MCD in experiments, one may first prepare the mixed state  $\rho_0$  with zero momentum and then evolve it in two different symmetric time frames and measure the shift of its center over a different number of driving periods in each time frame. Equations (18) and (17) can then be used to predict the topological winding numbers of the corresponding non-Hermitian Floquet system.

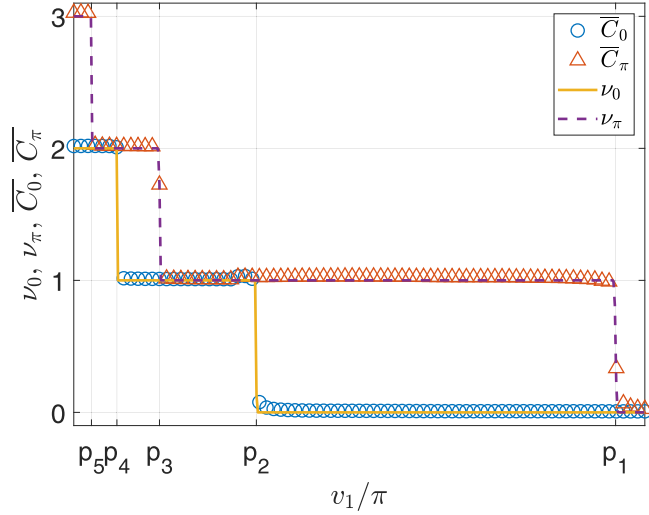


FIG. 6. The MCDs  $\bar{C}_0 = |\bar{C}_1 + \bar{C}_2|$  (blue circles) and  $\bar{C}_\pi = |\bar{C}_1 - \bar{C}_2|$  (red triangles) and winding numbers  $\nu_0$  (yellow solid line) and  $\nu_\pi$  (purple dashed line) vs the imaginary part of the kicking strength  $K_1 = u_1 + iv_1$ . The system parameters are set as  $u_1 = 5.5\pi$  and  $K_2 = u_2 = 0.5\pi$  and the results for  $\bar{C}_0$  and  $\bar{C}_\pi$  are averaged over  $t = 50$  kicking periods. Here  $v_1 = p_5$  to  $v_1 = p_1$  correspond to gap closing points obtained from Eq. (14) with  $n = 5, 4, 3, 2, 1$ .

#### D. Edge states and bulk-edge correspondence

The bulk-edge correspondence relates the number of topological edge states to the bulk topological invariant of the considered system. It forms an important recipe in the characterization of topological phases both theoretically and experimentally. The bulk-edge correspondence in non-Hermitian systems can be more complicated [89,90] due to the existence of high-order exceptional points [91,92] and the so-called non-Hermitian skin effect [93]. In an earlier study it was

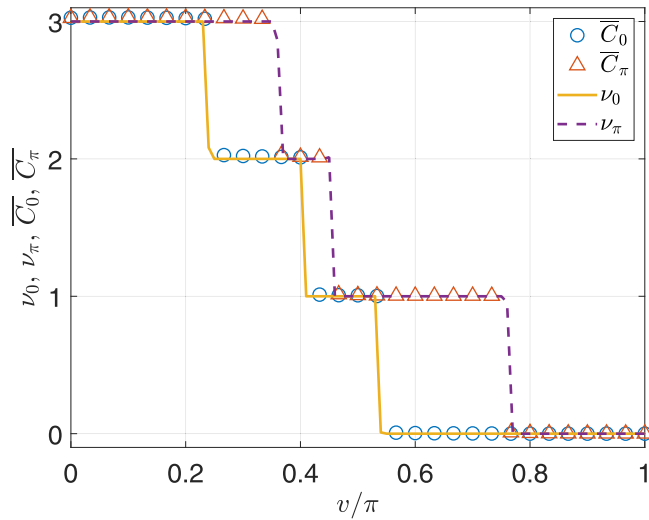


FIG. 7. The MCDs  $\bar{C}_0 = |\bar{C}_1 + \bar{C}_2|$  (blue circles) and  $\bar{C}_\pi = |\bar{C}_1 - \bar{C}_2|$  (red triangles) and winding numbers  $\nu_0$  (yellow solid line) and  $\nu_\pi$  (purple dashed line) vs the imaginary parts of kicking strengths  $K_1 = u_1 + iv$  and  $K_2 = u_2 + iv$ . The system parameters are set as  $u_1 = 0.5\pi$  and  $u_2 = 6.5\pi$  and the results for  $\bar{C}_0$  and  $\bar{C}_\pi$  are averaged over  $t = 50$  kicking periods.

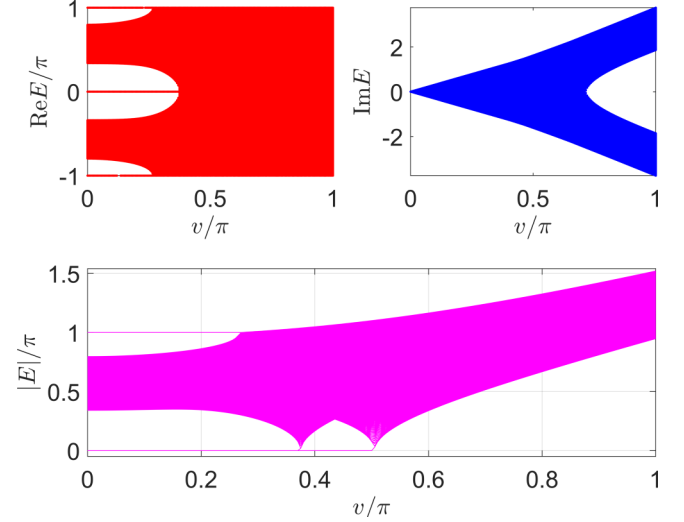


FIG. 8. Floquet spectrum of the NH ORDKR vs  $v$  under an OBC for kicking strengths  $K_1 = 5.5\pi + iv$  and  $K_2 = 0.5\pi + iv$ . The number of unit cells is chosen as  $N = 4000$  in the calculation.

shown that the bulk-edge correspondence can be recovered in non-Hermitian Floquet systems under appropriate conditions [74]. Below we demonstrate that the bulk-edge correspondence also holds in the NH ORDKR.

For the ORDKR, the lattice is defined in momentum space, where it is not straightforward to take an OBC and investigate the properties of edge states. To study the bulk-edge correspondence in the NH ORDKR, we can map its Hamiltonian to a periodically quenched lattice in position space. The resulting Floquet operator, according to Eqs. (A8)–(A10), can be expressed as

$$\begin{aligned} \hat{U} = & \exp\left(i\frac{\pi}{4} \sum_n |n\rangle\langle n|\sigma_z\right) \\ & \times \exp\left(-i\frac{K_2}{2} \sum_n (|n\rangle\langle n|\sigma_+ + |n\rangle\langle n+1|\sigma_- + \text{H.c.})\right) \\ & \times \exp\left(-i\frac{\pi}{4} \sum_n |n\rangle\langle n|\sigma_z\right) \\ & \times \exp\left(-i\frac{K_1}{2} \sum_n i(|n\rangle\langle n|\sigma_+ + |n\rangle\langle n+1|\sigma_- - \text{H.c.})\right), \end{aligned} \quad (19)$$

where  $n$  is now interpreted as the unit cell index of a real-space lattice and the Pauli matrices operate in the space of its sublattices. In this periodically quenched lattice model, the complex potentials  $K_1$  and  $K_2$  can be realized by introducing nonreciprocal hoppings and on-site gain or loss inside a unit cell and among nearest-neighbor unit cells. The implementation of these effects should be within reach in current photonic-based experimental setups [94].

The quasienergy spectrum and edge states of  $\hat{U}$  can now be obtained by solving the Floquet eigenvalue equation  $\hat{U}|\psi\rangle = e^{-iE}|\psi\rangle$  under the OBC. In Fig. 8 we show the Floquet spectrum of  $\hat{U}$  for  $u_1 = 5.5\pi$ ,  $u_2 = 0.5\pi$ , and  $v_1 = v_2 = v$ . In

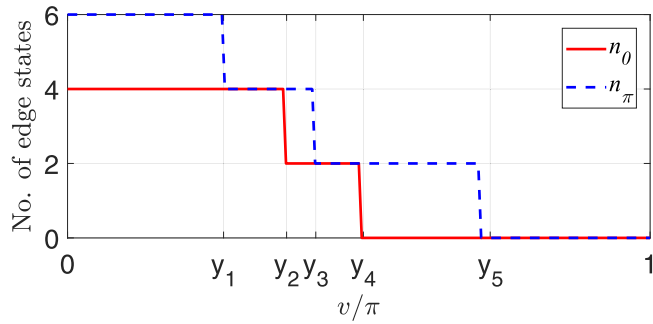


FIG. 9. Number of edge states at quasienergies 0 ( $n_0$ ) and  $\pm\pi$  ( $n_\pi$ ) vs the imaginary parts of kicking strengths  $K_1 = u_1 + iv_1$  and  $K_2 = u_2 + iv_2$  in the NH ORDKR. The system parameters are chosen as  $u_1 = 5.5\pi$ ,  $u_2 = 0.5\pi$ , and  $v_1 = v_2 = v$ . The number of unit cells is  $N = 4000$ . The bulk Floquet spectrum is gapless at quasienergy 0 or  $\pi$  when  $v = y_1, y_2, y_3, y_4, y_5$ , as obtained from the conditions (C8) and (C9).

the bottom panel we observe edge states pinned at quasienergies 0 and  $\pi$  in different regimes of the parameter space, with their numbers changing when the quasienergy gap closes at  $E = 0$  or  $E = \pm\pi$ .

In Fig. 9 we further show the number of topological edge states  $n_0$  at quasienergy 0 (red solid line) and  $n_\pi$  at quasienergy  $\pm\pi$  (blue dashed line) by computing the inverse participation ratio, with the same parameter choices as in Fig. 8. Here  $y_1 \sim y_5$  along the  $v$  axis corresponds to the gap closing points of the bulk quasienergy spectrum obtained from Eq. (11). We see that each time the gap closes at quasienergy 0 ( $\pi$ ),  $n_0$  ( $n_\pi$ ) will get a quantized change by 2, corresponding to a topological phase transition with winding number  $\nu_0$  ( $\nu_\pi$ ) changing by 1. In other regions, the bulk-edge correspondence described by the relations

$$n_0 = 2\nu_0, \quad n_\pi = 2\nu_\pi \quad (20)$$

holds as in Hermitian Floquet systems, with a small deviation around  $y_5$  due to finite-size effects. Equation (20) has also been checked numerically in other parameter regimes of the NH ORDKR, with similar results obtained. Therefore, we conclude that the bulk-edge correspondence in the NH ORDKR, as described by Eq. (20), holds in the same way as in the Hermitian ORDKR. Experimentally, the non-Hermitian Floquet topological edge states have been observed in photonic quantum walks [94]. We expect the relation (20) of the NH ORDKR to be verifiable in similar experimental setups.

#### IV. CONCLUSION

In this work we investigated Floquet topological phases in a non-Hermitian extension of the double-kicked rotor, which is a prototypical example of a dynamical kicking system. Under the on-resonance condition, the system possesses rich non-Hermitian Floquet topological phases protected by chiral symmetry. The topological phase diagram of the NH ORDKR was obtained, with each of its phase being characterized by a pair of integer winding numbers. These winding numbers could be detected dynamically by measuring the mean chiral displacement in two symmetric time frames. Furthermore, by

mapping our model to a periodically quenched lattice, we found its topological edge states. The number of these states at quasienergies 0 and  $\pm\pi$  in each topological phase is precisely counted by the winding numbers of bulk states, revealing the bulk-edge correspondence of the NH ORDKR.

In future studies, more fruitful topological structures are expected to appear in non-Hermitian dynamical kicking systems after introducing spin degrees of freedom and many-body interactions. Interesting examples include the recently discovered Floquet non-Hermitian skin effect [95] in momentum space and the non-Hermitian counterpart of Floquet topological time crystals [47]. New schemes that go beyond the existing 38-fold way for classification of static non-Hermitian topological phases [96,97] should be required to achieve a full characterization of these non-Hermitian Floquet states [98]. On the application side, the mean chiral displacement proposed in this work could assist the future experimental detection of topological invariants in non-Hermitian Floquet systems. Furthermore, with the promising proposal of Floquet topological quantum computing [47] and Floquet quantum state transfer [99], it would be interesting to investigate the potential of the Floquet topological edge states found in this work in achieving quantum computing and quantum information transfer against environmental effects that can be modeled by non-Hermitian Hamiltonians.

#### ACKNOWLEDGMENTS

L.Z. acknowledges J. Gong and B. Qu for helpful comments. This work was supported by the National Natural Science Foundation of China (Grant No. 11905211), the Young Talents Project at Ocean University of China (Grants No. 861801013196 and No. 841912009), and the Applied Research Project of Postdoctoral Fellows in Qingdao (Grant No. 861905040009).

#### APPENDIX A: FLOQUET OPERATOR IN DIFFERENT REPRESENTATIONS

The Floquet operator of the NH ORDKR, as given by Eq. (3), can be expressed in the momentum lattice representation as follows. We first write its component terms as

$$e^{\pm i(\pi/2)\hat{n}^2} = e^{\pm i(\pi/4)} \exp \left( \pm i(\pi/4) \sum_{\ell} (|2\ell - 1\rangle\langle 2\ell - 1| - |2\ell\rangle\langle 2\ell|) \right), \quad (A1)$$

$$e^{-iK_1 \cos(\hat{x} + \beta)} = \exp \left( -i(K_1/2) \sum_{\ell} (e^{i\beta} |2\ell - 1\rangle\langle 2\ell| + e^{i\beta} |2\ell\rangle\langle 2\ell + 1| + \text{H.c.}) \right), \quad (A2)$$

$$e^{-iK_2 \cos(\hat{x})} = \exp \left( -i(K_2/2) \sum_{\ell} (|2\ell - 1\rangle\langle 2\ell| + |2\ell\rangle\langle 2\ell + 1| + \text{H.c.}) \right), \quad (A3)$$

where the resolution identity  $I = \sum_{\ell} |\ell\rangle\langle \ell|$  has been inserted to arrive at the expansions. Since Eq. (3) is invariant under

the translation over two sites in momentum space, we could decompose the momentum space lattice into two chains containing only odd and even sites, denoted by sublattice indices  $a$  and  $b$ , respectively. A unit cell of the momentum space lattice now contains two sublattice sites and we can introduce Pauli matrices in the sublattice representation as

$$\sigma_x = |a\rangle\langle b| + |b\rangle\langle a|, \quad (\text{A4})$$

$$\sigma_y = i(|b\rangle\langle a| - |a\rangle\langle b|), \quad (\text{A5})$$

$$\sigma_z = |a\rangle\langle a| - |b\rangle\langle b|. \quad (\text{A6})$$

The sublattice raising and lower operators can also be expressed as

$$\sigma_{\pm} = \frac{\sigma_x + i\sigma_y}{2}. \quad (\text{A7})$$

In this bipartite lattice representation, Eqs. (A1)–(A3) can be written as

$$e^{\pm(\pi/2)\hat{n}^2} = e^{\pm i(\pi/4)} \exp\left(\pm i\frac{\pi}{4} \sum_n |n\rangle\langle n| \sigma_z\right), \quad (\text{A8})$$

$$e^{-iK_1 \cos(\hat{x}+\beta)} = \exp\left(-i\frac{K_1}{2} \sum_n (e^{i\beta} |n\rangle\langle n| \sigma_+ + e^{i\beta} |n\rangle\langle n+1| \sigma_- + \text{H.c.})\right), \quad (\text{A9})$$

$$e^{-iK_2 \cos(\hat{x})} = \exp\left(-i\frac{K_2}{2} \sum_n (|n\rangle\langle n| \sigma_+ + |n\rangle\langle n+1| \sigma_- + \text{H.c.})\right), \quad (\text{A10})$$

where  $n$  is the unit cell index. Performing the Fourier transforms  $|n\rangle = \sum_{\theta} e^{-in\theta} |\theta\rangle$  and  $\langle n| = \sum_{\theta} e^{in\theta} \langle\theta|$  on Eqs. (A8)–(A10) and choosing  $\beta = \frac{\pi}{2}$ , we arrive at

$$e^{\pm(\pi/2)\hat{n}^2} = e^{\pm i(\pi/4)} \exp\left(\pm i\frac{\pi}{4} \sum_{\theta} |\theta\rangle\langle\theta| \sigma_z\right), \quad (\text{A11})$$

$$e^{-iK_1 \cos(\hat{x}+\beta)} = \exp\left(-i\frac{K_1}{2} \sum_{\theta} |\theta\rangle\langle\theta| (i\sigma_+ + e^{i\theta} \sigma_- + \text{H.c.})\right), \quad (\text{A12})$$

$$e^{-iK_2 \cos(\hat{x})} = \exp\left(-i\frac{K_2}{2} \sum_{\theta} |\theta\rangle\langle\theta| (\sigma_+ + e^{i\theta} \sigma_- + \text{H.c.})\right). \quad (\text{A13})$$

Combing these terms in sequential order and using Eq. (A7), we obtain the Floquet operator of the NH ORDKR in the form  $\hat{U} = \sum_{\theta} U(\theta) |\theta\rangle\langle\theta|$ , with

$$U(\theta) = e^{+i(\pi/4)\sigma_z} e^{-i(K_2/2)[(1+\cos\theta)\sigma_x + \sin\theta\sigma_y]} \times e^{-i(\pi/4)\sigma_z} e^{+i(K_1/2)[\sin\theta\sigma_x + (1-\cos\theta)\sigma_y]}. \quad (\text{A14})$$

Finally, using trigonometric relations  $\sin\theta = 2\sin\frac{\theta}{2}\cos\frac{\theta}{2}$  and  $\cos\theta = 2\cos^2\frac{\theta}{2} - 1 = 1 - 2\sin^2\frac{\theta}{2}$ , we arrive at Eq. (5).

Further,  $U(\theta)$  can be expressed in the two symmetric time frames as discussed in the main text. To do so, we first shift the starting time of the evolution to the start of the second half of

the driving period and split the kick  $e^{-i(K_2/2)[(1+\cos\theta)\sigma_x + \sin\theta\sigma_y]}$  into two ‘‘half kicks’’ at the start and end of the shifted evolution. The resulting Floquet operator in this new time frame is given by

$$U_1(\theta) = e^{-i(K_2/2)[\cos(\theta/2)\sigma_x + \sin(\theta/2)\sigma_y]} \times e^{-i(\pi/4)\sigma_z} e^{+iK_1[\cos(\theta/2)\sigma_x + \sin(\theta/2)\sigma_y]} e^{+i(\pi/4)\sigma_z} \times e^{-i(K_2/2)[\cos(\theta/2)\sigma_x + \sin(\theta/2)\sigma_y]}. \quad (\text{A15})$$

Similarly, by splitting  $e^{+iK_1[\cos(\theta/2)\sigma_x + \sin(\theta/2)\sigma_y]}$  into two half kicks and shifting one of them to the end of the evolution,  $U(\theta)$  in Eq. (A14) becomes

$$U_2(\theta) = e^{+i(K_1/2)[\cos(\theta/2)\sigma_x + \sin(\theta/2)\sigma_y]} \times e^{+i(\pi/4)\sigma_z} e^{-iK_2[\cos(\theta/2)\sigma_x + \sin(\theta/2)\sigma_y]} e^{-i(\pi/4)\sigma_z} \times e^{+i(K_1/2)[\cos(\theta/2)\sigma_x + \sin(\theta/2)\sigma_y]}. \quad (\text{A16})$$

It is clear that both  $U_1(\theta)$  and  $U_2(\theta)$  are related to  $U(\theta)$  by similarity transformations. Finally, using the transformations  $e^{\mp i(\pi/4)\sigma_z} \sigma_x e^{\pm i(\pi/4)\sigma_z} = \pm \sigma_y$  and  $e^{\mp i(\pi/4)\sigma_z} \sigma_y e^{\pm i(\pi/4)\sigma_z} = \mp \sigma_x$ , Eqs. (A15) and (A16) simplify to Eqs. (7) and (8), respectively.

## APPENDIX B: EXPLICIT EXPRESSIONS OF THE FLOQUET OPERATORS

Using the Euler formula  $e^{i\phi\mathbf{n}\cdot\boldsymbol{\sigma}} = \cos\phi + i\sin\phi\mathbf{n}\cdot\boldsymbol{\sigma}$ , we can expand each exponential of Eqs. (7) and (8). The resulting terms can be recombined to give

$$U_1(\theta) = \cos\mathcal{K}_1 \cos\mathcal{K}_2 - i\left[\cos\frac{\theta}{2} \cos\mathcal{K}_1 \sin\mathcal{K}_2 + \sin\frac{\theta}{2} \sin\mathcal{K}_1\right] \sigma_x - i\left[\sin\frac{\theta}{2} \cos\mathcal{K}_1 \sin\mathcal{K}_2 - \cos\frac{\theta}{2} \sin\mathcal{K}_1\right] \sigma_y \quad (\text{B1})$$

and

$$U_2(\theta) = \cos\mathcal{K}_1 \cos\mathcal{K}_2 - i\left[-\cos\frac{\theta}{2} \sin\mathcal{K}_1 \cos\mathcal{K}_2 + \sin\frac{\theta}{2} \sin\mathcal{K}_2\right] \sigma_x - i\left[-\sin\frac{\theta}{2} \sin\mathcal{K}_1 \cos\mathcal{K}_2 - \cos\frac{\theta}{2} \sin\mathcal{K}_2\right] \sigma_y. \quad (\text{B2})$$

By setting  $\cos[E(\theta)] = \cos\mathcal{K}_1 \cos\mathcal{K}_2$ , it is straightforward to see that  $E(\theta) = \arccos(\cos\mathcal{K}_1 \cos\mathcal{K}_2)$ , and Eqs. (B1) and (B2) have the form of Eq. (10), with

$$n_{1x} = \frac{\cos\frac{\theta}{2} \cos\mathcal{K}_1 \sin\mathcal{K}_2 + \sin\frac{\theta}{2} \sin\mathcal{K}_1}{\sin E(\theta)}, \quad (\text{B3})$$

$$n_{1y} = \frac{\sin\frac{\theta}{2} \cos\mathcal{K}_1 \sin\mathcal{K}_2 - \cos\frac{\theta}{2} \sin\mathcal{K}_1}{\sin E(\theta)}, \quad (\text{B4})$$

$$n_{2x} = \frac{-\cos\frac{\theta}{2} \sin\mathcal{K}_1 \cos\mathcal{K}_2 + \sin\frac{\theta}{2} \sin\mathcal{K}_2}{\sin E(\theta)}, \quad (\text{B5})$$

$$n_{2y} = \frac{-\sin\frac{\theta}{2} \sin\mathcal{K}_1 \cos\mathcal{K}_2 - \cos\frac{\theta}{2} \sin\mathcal{K}_2}{\sin E(\theta)}. \quad (\text{B6})$$



### APPENDIX C: GAPLESS CONDITIONS

We present derivation details for the gap closing conditions. Using the shorthand notation

$$u_1 \equiv u_1 \sin \frac{\theta}{2}, \quad u_2 \equiv u_2 \cos \frac{\theta}{2}, \quad (\text{C1})$$

$$v_1 \equiv v_1 \sin \frac{\theta}{2}, \quad v_2 \equiv v_2 \cos \frac{\theta}{2}, \quad (\text{C2})$$

we can express the gap closing condition as

$$\cos E = \cos(u_1 + iv_1) \cos(u_2 + iv_2) = \pm 1. \quad (\text{C3})$$

When  $v_1 \neq 0$  and  $v_2 = 0$ , this condition is equivalent to

$$\cos u_1 \cosh v_1 \cos u_2 = \pm 1, \quad (\text{C4})$$

$$\sin u_1 \sinh v_1 \cos u_2 = 0. \quad (\text{C5})$$

It is clear that to satisfy both equations,  $\cos u_2$  cannot be zero. Furthermore, if  $\sinh v_1 = 0$ , we must have  $\sin \frac{\theta}{2} = 0$ , and Eq. (C5) will be satisfied only if  $\cos(u_2) = \pm 1$ , which is a very special condition that is irrelevant to the value of  $v_1$ . Therefore, Eq. (C5) is generally satisfied if  $\sin u_1 = 0$ , yielding  $\sin \frac{\theta}{2} = \frac{n\pi}{u_1}$  for  $n\pi \leq u_1$  with  $n \in \mathbb{N}$ . Plugging this relation into Eq. (C4) and regrouping the relevant terms, we obtain Eq. (14). Equation (15) can be derived in a similar manner.

In more general situations, the gapless condition can be extracted numerically. We first separate Eq. (C3) into its real part  $f$  and imaginary part  $g$ . Expressed in terms of  $f$  and  $g$ , the Floquet spectrum is gapless when

$$\begin{aligned} \pm 1 = f &= \cos u_1 \cos u_2 \cosh v_1 \cosh v_2 \\ &\quad - \sin u_1 \sin u_2 \sinh v_1 \sinh v_2 \end{aligned} \quad (\text{C6})$$

and

$$\begin{aligned} 0 = g &= \cos u_1 \sin u_2 \cosh v_1 \sinh v_2 \\ &\quad + \sin u_1 \cos u_2 \sinh v_1 \cosh v_2. \end{aligned} \quad (\text{C7})$$

Using  $f$  and  $g$ , we could further introduce a pair of functions  $(\Delta_0, \Delta_\pi)$  to characterize the size of spectral gaps at quasienergies  $E = 0$  and  $E = \pm\pi$ , respectively. Explicitly, these functions are defined as

$$\Delta_0 = \sqrt{(f-1)^2 + g^2}, \quad (\text{C8})$$

$$\Delta_\pi = \sqrt{(f+1)^2 + g^2}. \quad (\text{C9})$$

Therefore, the spectrum becomes gapless at the center (edge) of the quasienergy Brillouin zone if  $\Delta_0 = 0$  ( $\Delta_\pi = 0$ ).

### APPENDIX D: DERIVATION OF THE MEAN CHIRAL DISPLACEMENT

We provide derivation details for Eq. (17) in this Appendix. In the definition of chiral displacement by Eq. (16), we can insert the identity in the lattice representation to yield

$$\begin{aligned} &\text{Tr}[\rho_0 \hat{U}_\alpha^{\dagger t} (\hat{n} \otimes \Gamma) \hat{U}_\alpha^t] \\ &= \frac{1}{2} \sum_n \sum_{s,s'=a,b} n \langle 0|s \langle \hat{U}_\alpha^{\dagger t} |n \rangle \Gamma |s' \rangle \langle s' | \langle n | \hat{U}_\alpha^t |0 \rangle |s \rangle. \end{aligned} \quad (\text{D1})$$

Expressing  $\hat{U}_\alpha$  and  $\hat{U}_\alpha^\dagger$  in the quasiposition (or quasimomentum for real-space lattices) representation as  $\hat{U}_\alpha = \sum_\theta |\theta\rangle U_\alpha(\theta) \langle \theta|$  and  $\hat{U}_\alpha^\dagger = \sum_\theta |\theta\rangle \tilde{U}_\alpha^\dagger(\theta) \langle \theta|$ , with  $U_\alpha(\theta)$  and  $\tilde{U}_\alpha^\dagger(\theta)$  being  $2 \times 2$  matrices in the sublattice representation, we further obtain

$$\begin{aligned} \text{Tr}[\rho_0 \hat{U}_\alpha^{\dagger t} (\hat{n} \otimes \Gamma) \hat{U}_\alpha^t] &= \frac{1}{2} \sum_n \sum_{\theta\theta'} n \langle 0|\theta\rangle \langle \theta|n\rangle \langle n|\theta'\rangle \langle \theta'|0\rangle \\ &\quad \times \text{Tr}[\tilde{U}_\alpha^{\dagger t}(\theta) \Gamma U_\alpha^t(\theta')], \end{aligned} \quad (\text{D2})$$

where the trace is now taken over the sublattice degrees of freedom. Using the Fourier transform relations

$$\begin{aligned} |\theta\rangle &= \frac{1}{\sqrt{N}} \sum_n e^{i\theta n} |n\rangle, \\ |n\rangle &= \frac{1}{\sqrt{N}} \sum_\theta e^{-i\theta n} |\theta\rangle, \\ \langle n|\theta\rangle &= \frac{1}{\sqrt{N}} e^{i\theta n}, \end{aligned} \quad (\text{D3})$$

we can simplify the numerator to

$$\begin{aligned} &\text{Tr}[\rho_0 \hat{U}_\alpha^{\dagger t} (\hat{n} \otimes \Gamma) \hat{U}_\alpha^t] \\ &= \frac{1}{2} \sum_n \sum_{\theta\theta'} n \frac{1}{N^2} e^{in(\theta'-\theta)} \text{Tr}[\tilde{U}_\alpha^{\dagger t}(\theta) \Gamma U_\alpha^t(\theta')]. \end{aligned} \quad (\text{D4})$$

Using the relation

$$\frac{1}{N} \sum_n n e^{i(\theta'-\theta)n} = i\partial_\theta \frac{1}{N} \sum_n e^{i(\theta'-\theta)n} = i\partial_\theta \delta_{\theta\theta'}, \quad (\text{D5})$$

we find

$$\begin{aligned} &\text{Tr}[\rho_0 \hat{U}_\alpha^{\dagger t} (\hat{n} \otimes \Gamma) \hat{U}_\alpha^t] \\ &= \frac{1}{2} \sum_{\theta\theta'} \frac{1}{N} i\partial_\theta \delta_{\theta\theta'} \text{Tr}[\tilde{U}_\alpha^{\dagger t}(\theta) \Gamma U_\alpha^t(\theta')]. \end{aligned} \quad (\text{D6})$$

In the continuous limit ( $N \rightarrow \infty$ ), we have  $\delta_{\theta\theta'} \rightarrow \frac{2\pi}{N} \delta(\theta - \theta')$  and  $\sum_{\theta,\theta'} \rightarrow N^2 \int_{-\pi}^{\pi} \frac{d\theta}{2\pi} \int_{-\pi}^{\pi} \frac{d\theta'}{2\pi}$ . Combining this into Eq. (D6) then leads to

$$\begin{aligned} C_\alpha(t) &= \text{Tr}[\rho_0 \hat{U}_\alpha^{\dagger t} (\hat{n} \otimes \Gamma) \hat{U}_\alpha^t] \\ &= \frac{1}{2} \int_{-\pi}^{\pi} \frac{d\theta}{2\pi} \text{Tr}[\tilde{U}_\alpha^{\dagger t}(\theta) \Gamma i\partial_\theta U_\alpha^t(\theta)]. \end{aligned} \quad (\text{D7})$$

Inserting the normalization factor  $\frac{1}{2} \text{Tr}[\tilde{U}_\alpha^{\dagger t}(\theta) U_\alpha^t(\theta)]$  at each  $\theta$  (since the evolution will change the normal of the state) and taking the long-time average  $\lim_{t \rightarrow \infty} \frac{1}{t} \sum_{t'=1}^t$ , we obtain the expression for MCD as

$$\bar{C}_\alpha = \lim_{t \rightarrow \infty} \frac{1}{t} \sum_{t'=1}^t \int_{-\pi}^{\pi} \frac{d\theta}{2\pi} \frac{\text{Tr}[\tilde{U}_\alpha^{\dagger t'}(\theta) \Gamma i\partial_\theta U_\alpha^{t'}(\theta)]}{\text{Tr}[\tilde{U}_\alpha^{\dagger t'}(\theta) U_\alpha^{t'}(\theta)]}. \quad (\text{D8})$$

For the NH ORDKR, we have  $\Gamma = \sigma_z$ ,  $U_\alpha(\theta) = e^{-iE(\mathbf{n}_\alpha \cdot \sigma)}$ , and  $\tilde{U}_\alpha^\dagger(\theta) = e^{+iE^*(\mathbf{n}_\alpha \cdot \sigma)}$ . Plugging these into Eq. (D8), the numerator and denominator become, respectively,

$$\text{Tr}[\tilde{U}_\alpha^{\dagger t'}(\theta) U_\alpha^{t'}(\theta)] = 2[|\cos(Et')|^2 + |\sin(Et')|^2], \quad (\text{D9})$$

$$\text{Tr}[\tilde{U}_\alpha^{\dagger t'}(\theta) \Gamma i\partial_\theta U_\alpha^{t'}(\theta)] = 2|\sin(Et')|^2 (\mathbf{n}_\alpha \times \partial_\theta \mathbf{n}_\alpha)_z. \quad (\text{D10})$$

Combining these into Eq. (D8), we finally obtain Eq. (17).

- [1] P. Leboeuf, J. Kurchan, M. Feingold, and D. P. Arovas, *Phys. Rev. Lett.* **65**, 3076 (1990).
- [2] G. Casati, B. V. Chirikov, F. M. Izrailev, and J. Ford, in *Stochastic Behaviour in Classical and Quantum Hamiltonian Systems*, edited by G. Casati and J. Ford, Lecture Notes in Physics Vol. 93 (Springer, New York, 1979).
- [3] G. Casati and B. V. Chirikov, *Quantum Chaos: Between Order and Disorder* (Cambridge University Press, New York, 1995).
- [4] H. Ammann, R. Gray, I. Shvachuck, and N. Christensen, *Phys. Rev. Lett.* **80**, 4111 (1998); B. G. Klappauf, W. H. Oskay, D. A. Steck, and M. G. Raizen, *ibid.* **81**, 1203 (1998).
- [5] J. Chabé, G. Lemarié, B. Grémaud, D. Delande, P. Szriftgiser, and J. C. Garreau, *Phys. Rev. Lett.* **101**, 255702 (2008).
- [6] D. H. White, S. K. Ruddell, and M. D. Hoogerland, *Phys. Rev. A* **88**, 063603 (2013).
- [7] F. M. Izrailev, *Phys. Rep.* **196**, 299 (1990); M. G. Raizen, *Adv. At. Mol. Opt. Phys.* **41**, 43 (1999); I. Dana, *Can. J. Chem.* **92**, 77 (2014); M. Sadgrove and S. Wimberger, *Adv. At. Mol. Opt. Phys.* **60**, 315 (2011).
- [8] J. Wang and J. Gong, *Phys. Rev. A* **77**, 031405(R) (2008); J. Wang, A. S. Mouritzen, and J. Gong, *J. Mod. Opt.* **56**, 722 (2009).
- [9] D. R. Hofstadter, *Phys. Rev. B* **14**, 2239 (1976).
- [10] D. Y. H. Ho and J. Gong, *Phys. Rev. Lett.* **109**, 010601 (2012); *Phys. Rev. B* **90**, 195419 (2014).
- [11] I. Dana, *Phys. Lett. A* **197**, 413 (1995).
- [12] H. Wang, D. Y. H. Ho, W. Lawton, J. Wang, and J. Gong, *Phys. Rev. E* **88**, 052920 (2013).
- [13] J. P. Dahlhaus, J. M. Edge, J. Tworzydło, and C. W. J. Beenakker, *Phys. Rev. B* **84**, 115133 (2011).
- [14] Y. Chen and C. Tian, *Phys. Rev. Lett.* **113**, 216802 (2014); C. Tian, Y. Chen, and J. Wang, *Phys. Rev. B* **93**, 075403 (2016).
- [15] L. Zhou and J. Gong, *Phys. Rev. A* **97**, 063603 (2018).
- [16] T. Oka and H. Aoki, *Phys. Rev. B* **79**, 081406(R) (2009).
- [17] N. H. Lindner, G. Refael, and V. Galitski, *Nat. Phys.* **7**, 490 (2011).
- [18] T. Kitagawa, T. Oka, A. Brataas, L. Fu, and E. Demler, *Phys. Rev. B* **84**, 235108 (2011).
- [19] Q.-J. Tong, J.-H. An, J. Gong, H.-G. Luo, and C. H. Oh, *Phys. Rev. B* **87**, 201109(R) (2013).
- [20] L. Zhou, H. Wang, D. Y. H. Ho, and J. Gong, *Eur. Phys. J. B* **87**, 204 (2014).
- [21] T.-S. Xiong, J. Gong, and J.-H. An, *Phys. Rev. B* **93**, 184306 (2016).
- [22] Á. Gómez-León and G. Platero, *Phys. Rev. Lett.* **110**, 200403 (2013).
- [23] J. Cayssol, B. Dóra, F. Simon, and R. Moessner, *Phys. Status Solidi Rapid Res. Lett.* **7**, 101 (2013).
- [24] M. Thakurathi, A. A. Patel, D. Sen, and A. Dutta, *Phys. Rev. B* **88**, 155133 (2013).
- [25] A. G. Grushin, Á. Gómez-León, and T. Neupert, *Phys. Rev. Lett.* **112**, 156801 (2014).
- [26] R. Wang, B. Wang, R. Shen, L. Sheng, and D. Y. Xing, *Europhys. Lett.* **105**, 17004 (2014).
- [27] P. Titum, N. H. Lindner, M. C. Rechtsman, and G. Refael, *Phys. Rev. Lett.* **114**, 056801 (2015).
- [28] J. Klinovaja, P. Stano, and D. Loss, *Phys. Rev. Lett.* **116**, 176401 (2016); M. Thakurathi, D. Loss, and J. Klinovaja, *Phys. Rev. B* **95**, 155407 (2017).
- [29] T. Kitagawa, E. Berg, M. Rudner, and E. Demler, *Phys. Rev. B* **82**, 235114 (2010).
- [30] L. Jiang, T. Kitagawa, J. Alicea, A. R. Akhmerov, D. Pekker, G. Refael, J. I. Cirac, E. Demler, M. D. Lukin, and P. Zoller, *Phys. Rev. Lett.* **106**, 220402 (2011).
- [31] A. Kundu and B. Seradjeh, *Phys. Rev. Lett.* **111**, 136402 (2013).
- [32] R. W. Bomantara, G. N. Raghava, L. Zhou, and J. Gong, *Phys. Rev. E* **93**, 022209 (2016); R. W. Bomantara and J. Gong, *Phys. Rev. B* **94**, 235447 (2016).
- [33] M. Lababidi, I. I. Satija, and E. Zhao, *Phys. Rev. Lett.* **112**, 026805 (2014); Z. Zhou, I. I. Satija, and E. Zhao, *Phys. Rev. B* **90**, 205108 (2014).
- [34] M. D. Reichl and E. J. Mueller, *Phys. Rev. A* **89**, 063628 (2014).
- [35] Á. Gómez-León, P. Delplace, and G. Platero, *Phys. Rev. B* **89**, 205408 (2014).
- [36] M. S. Rudner, N. H. Lindner, E. Berg, and M. Levin, *Phys. Rev. X* **3**, 031005 (2013); P. Titum, E. Berg, M. S. Rudner, G. Refael, and N. H. Lindner, *ibid.* **6**, 021013 (2016).
- [37] I. C. Fulga and M. Maksymenko, *Phys. Rev. B* **93**, 075405 (2016).
- [38] L. Zhou, C. Chen, and J. Gong, *Phys. Rev. B* **94**, 075443 (2016).
- [39] J. K. Asbóth, *Phys. Rev. B* **86**, 195414 (2012); J. K. Asbóth and H. Obuse, *ibid.* **88**, 121406(R) (2013).
- [40] M. Rodriguez-Vega and B. Seradjeh, *Phys. Rev. Lett.* **121**, 036402 (2018).
- [41] H. H. Yap, L. Zhou, J.-S. Wang, and J. Gong, *Phys. Rev. B* **96**, 165443 (2017).
- [42] H. H. Yap, L. Zhou, C. H. Lee, and J. Gong, *Phys. Rev. B* **97**, 165142 (2018).
- [43] L. Zhou and J. Gong, *Phys. Rev. B* **97**, 245430 (2018).
- [44] L. Li, C. H. Lee, and J. Gong, *Phys. Rev. Lett.* **121**, 036401 (2018).
- [45] T. Oka and S. Kitamura, *Annu. Rev. Condens. Matter Phys.* **10**, 387 (2019).
- [46] A. Eckardt, *Rev. Mod. Phys.* **89**, 011004 (2017).
- [47] R. W. Bomantara and J. Gong, *Phys. Rev. Lett.* **120**, 230405 (2018); *Phys. Rev. B* **98**, 165421 (2018).
- [48] F. Nathan and M. S. Rudner, *New J. Phys.* **17**, 125014 (2015).
- [49] R. Roy and F. Harper, *Phys. Rev. B* **94**, 125105 (2016); **96**, 155118 (2017).
- [50] S. Yao, Z. Yan, and Z. Wang, *Phys. Rev. B* **96**, 195303 (2017).
- [51] G. Jotzu, M. Messer, R. Desbuquois, M. Lebrat, T. Uehlinger, D. Greif, and T. Esslinger, *Nature (London)* **515**, 237 (2014); M. Aidelsburger, M. Lohse, C. Schweizer, M. Atala, J. T. Barreiro, S. Nascimbène, N. R. Cooper, I. Bloch, and N. Goldman, *Nat. Phys.* **11**, 162 (2015).
- [52] N. Fläschner, B. S. Rem, M. Tarnowski, Vogel, D.-S. Lühmann, K. Sengstock, and C. Weitenberg, *Science* **352**, 1091 (2016).
- [53] T. Kitagawa, M. A. Broome, A. Fedrizzi, M. S. Rudner, E. Berg, I. Kassal, A. Aspuru-Guzik, E. Demler, and A. G. White, *Nat. Commun.* **3**, 882 (2012).
- [54] M. C. Rechtsman, J. M. Zeuner, Y. Plotnik, Y. Lumer, D. Podolsky, F. Dreisow, S. Nolte, M. Segev, and A. Szameit, *Nature (London)* **496**, 196 (2013); W. Hu, J. C. Pillay, K. Wu, M. Pasek, P. P. Shum, and Y. D. Chong, *Phys. Rev. X* **5**, 011012 (2015).
- [55] L. J. Maczewsky, J. M. Zeuner, S. Nolte, and A. Szameit, *Nat. Commun.* **8**, 13756 (2017); S. Mukherjee, A. Spracklen, M. Valiente, E. Andersson, P. Ohberg, N. Goldman, and R. R. Thomson, *ibid.* **8**, 13918 (2017).

- [56] M. Xiao, G. Ma, Z. Yang, P. Sheng, Z. Q. Zhang, and C. T. Chan, *Nat. Phys.* **11**, 240 (2015); R. Süssstrunk and S. D. Huber, *Science* **349**, 47 (2015); R. Fleury, A. B. Khanikaev and A. Alù, *Nat. Commun.* **7**, 11744 (2016); R. Süssstrunk, P. Zimmermann, and S. D. Huber, *New J. Phys.* **19**, 015013 (2017).
- [57] Y. Peng, C. Qin, D. Zhao, Y. Shen, X. Xu, M. Bao, H. Jia, and X. Zhu, *Nat. Commun.* **7**, 13368 (2016).
- [58] V. M. M. Alvarez, J. E. B. Vargas, M. Berdakin, and L. E. F. Foa Torres, *Eur. Phys. J. Spec. Top.* **227**, 1295 (2018).
- [59] A. Ghatak and T. Das, *J. Phys.: Condens. Matter* **31**, 263001 (2019); arXiv:1907.07333.
- [60] C. Yuce, *Eur. Phys. J. D* **69**, 184 (2015); Z. Turkera, S. Tombuloglu, and C. Yuce, *Phys. Lett. A* **382**, 2013 (2018).
- [61] D. Kim, M. Ken, N. Kawakami, and H. Obuse, arXiv:1609.09650.
- [62] J. Gong and Q.-h. Wang, *Phys. Rev. A* **91**, 042135 (2015).
- [63] X.-Y. Lü, H. Jing, J.-Y. Ma, and Y. Wu, *Phys. Rev. Lett.* **114**, 253601 (2015).
- [64] Q. Bin, X.-Y. Lü, T.-S. Yin, Y. Li, and Y. Wu, *Phys. Rev. A* **99**, 033809 (2019).
- [65] M. S. Rudner and L. S. Levitov, *Phys. Rev. Lett.* **102**, 065703 (2009).
- [66] J. M. Zeuner, M. C. Rechtsman, Y. Plotnik, Y. Lumer, S. Nolte, M. S. Rudner, M. Segev, and A. Szameit, *Phys. Rev. Lett.* **115**, 040402 (2015).
- [67] K. Mochizuki, D. Kim, and H. Obuse, *Phys. Rev. A* **93**, 062116 (2016).
- [68] Y. Huang, Z.-q. Yin, and W. L. Yang, *Phys. Rev. A* **94**, 022302 (2016).
- [69] T. Rakovszky, J. K. Asbóth, and A. Alberti, *Phys. Rev. B* **95**, 201407(R) (2017).
- [70] L. Xiao, X. Zhan, Z. H. Bian, K. K. Wang, X. Zhang, X. P. Wang, J. Li, K. Mochizuki, D. Kim, N. Kawakami, W. Yi, H. Obuse, B. C. Sanders, and P. Xue, *Nat. Phys.* **13**, 1117 (2017); L. Xiao, X. Qiu, K. Wang, Z. Bian, X. Zhan, H. Obuse, B. C. Sanders, W. Yi, and P. Xue, *Phys. Rev. A* **98**, 063847 (2018).
- [71] T. Chen, B. Wang, and X. Zhang, *Phys. Rev. A* **97**, 052117 (2018).
- [72] A. K. Harter, A. Saxena, and Y. N. Joglekar, *Sci. Rep.* **8**, 12065 (2018).
- [73] K. Wang, X. Qiu, L. Xiao, X. Zhan, Z. Bian, W. Yi, and P. Xue, *Phys. Rev. Lett.* **122**, 020501 (2019).
- [74] L. Zhou and J. Gong, *Phys. Rev. B* **98**, 205417 (2018).
- [75] S. Longhi, *Phys. Rev. A* **95**, 012125 (2017).
- [76] C. T. West, T. Kottos, and T. Prosen, *Phys. Rev. Lett.* **104**, 054102 (2010).
- [77] W.-L. Zhao, J. Wang, X. Wang, and P. Tong, *Phys. Rev. E* **99**, 042201 (2019).
- [78] P. H. Jones, M. M. Stocklin, G. Hur, and T. S. Monteiro, *Phys. Rev. Lett.* **93**, 223002 (2004).
- [79] G. Hur, C. E. Creffield, P. H. Jones, and T. S. Monteiro, *Phys. Rev. A* **72**, 013403 (2005); C. E. Creffield, S. Fishman, and T. S. Monteiro, *Phys. Rev. E* **73**, 066202 (2006); M. M. A. Stocklin and T. S. Monteiro, *ibid.* **74**, 026210 (2006); C. E. Creffield, G. Hur, and T. S. Monteiro, *Phys. Rev. Lett.* **96**, 024103 (2006); J. Reslen, C. E. Creffield, and T. S. Monteiro, *Phys. Rev. A* **77**, 043621 (2008).
- [80] G. G. Carlo, G. Benenti, G. Casati, S. Wimberger, O. Morsch, R. Mannella, and E. Arimondo, *Phys. Rev. A* **74**, 033617 (2006).
- [81] C. Ryu, M. F. Andersen, A. Vaziri, M. B. d'Arcy, J. M. Grossman, K. Helmerson, and W. D. Phillips, *Phys. Rev. Lett.* **96**, 160403 (2006); I. Talukdar, R. Shrestha, and G. S. Summy, *ibid.* **105**, 054103 (2010).
- [82] I. Dana, V. Ramareddy, I. Talukdar, and G. S. Summy, *Phys. Rev. Lett.* **100**, 024103 (2008); M. Sadgrove, M. Horikoshi, T. Sekimura, and K. Nakagawa, *ibid.* **99**, 043002 (2007).
- [83] F. L. Moore, J. C. Robinson, C. F. Bharucha, B. Sundaram, and M. G. Raizen, *Phys. Rev. Lett.* **75**, 4598 (1995); J. F. Kanem, S. Maneshi, M. Partlow, M. Spanner, and A. M. Steinberg, *ibid.* **98**, 083004 (2007); A. Ullah and M. D. Hoogerland, *Phys. Rev. E* **83**, 046218 (2011).
- [84] Y. Xu, S.-T. Wang, and L.-M. Duan, *Phys. Rev. Lett.* **118**, 045701 (2017).
- [85] S. Longhi, *Phys. Rev. A* **81**, 022102 (2010).
- [86] F. Cardano, A. D'Errico, A. Dauphin, M. Maffei, B. Piccirillo, C. de Lisio, G. D. Filippis, V. Cataudella, E. Santamato, L. Marrucci, M. Lewenstein, and P. Massignan, *Nat. Commun.* **8**, 15516 (2017); M. Maffei, A. Dauphin, F. Cardano, M. Lewenstein, and P. Massignan, *New J. Phys.* **20**, 013023 (2018).
- [87] E. J. Meier, F. A. An, A. Dauphin, M. Maffei, P. Massignan, T. L. Hughes, and B. Gadway, *Science* **362**, 929 (2018).
- [88] R. W. Bomantara, L. Zhou, J. Pan, and J. Gong, *Phys. Rev. B* **99**, 045441 (2019).
- [89] F. K. Kunst, E. Edvardsson, J. C. Budich, and E. J. Bergholtz, *Phys. Rev. Lett.* **121**, 026808 (2018).
- [90] D. S. Borgnia, A. J. Kruchkov, and R.-J. Slager, arXiv:1902.07217.
- [91] T. E. Lee, *Phys. Rev. Lett.* **116**, 133903 (2016).
- [92] D. J. Luitz and F. Piazza, *Phys. Rev. Research* **1**, 033051 (2019).
- [93] S. Yao and Z. Wang, *Phys. Rev. Lett.* **121**, 086803 (2018).
- [94] L. Xiao, T. Deng, K. Wang, G. Zhu, Z. Wang, W. Yi, and P. Xue, arXiv:1907.12566.
- [95] X. Zhang and J. Gong, arXiv:1909.10234.
- [96] H. Zhou and J. Y. Lee, *Phys. Rev. B* **99**, 235112 (2019).
- [97] K. Kawabata, K. Shiozaki, M. Ueda, and M. Sato, *Phys. Rev. X* **9**, 041015 (2019).
- [98] L. Zhou, arXiv:1909.10797.
- [99] S. Tan, R. W. Bomantara, and J. Gong, arXiv:1909.03646.